energies

MDPI

Article

Control-Informed Geometric Optimization of Wave Energy Converters: The Impact of Device Motion and Force Constraints

Paula B. Garcia-Rosa *, Giorgio Bacelli † and John V. Ringwood *

Received: 27 August 2015; Accepted: 23 November 2015; Published: 2 December 2015
Academic Editor: Jens Peter Kofoed

Centre for Ocean Energy Research, Maynooth University, Maynooth, Co. Kildare, Ireland
* Correspondence: paula.garciarosa@eeng.nuim.ie (P.B.G.-R.); john.ringwood@eeng.nuim.ie (J.V.R.); Tel.: +353-1-708-4766 (J.V.R.); Fax: +353-1-708-6027 (J.V.R.)
† Current Address: Water Power Technologies Department, Sandia National Laboratories, Albuquerque, NM 87123, USA; gbacelli@sandia.gov. (This work was completed while Giorgio Bacelli was affiliated with the Centre for Ocean Energy Research at Maynooth University).

Abstract: The energy cost for producing electricity via wave energy converters (WECs) is still not competitive with other renewable energy sources, especially wind energy. It is well known that energy maximising control plays an important role to improve the performance of WECs, allowing the energy conversion to be performed as economically as possible. The control strategies are usually subsequently employed on a device that was designed and optimized in the absence of control for the prevailing sea conditions in a particular location. If an optimal unconstrained control strategy, such as pseudo-spectral optimal control (PSOC), is adopted, an overall optimized system can be obtained no matter whether the control design is incorporated at the geometry optimization stage or not. Nonetheless, strategies, such as latching control (LC), must be incorporated at the optimization design stage of the WEC geometry if an overall optimized system is to be realised. In this paper, the impact of device motion and force constraints in the design of control-informed optimized WEC geometries is addressed. The aim is to verify to what extent the constraints modify the connection between the control and the optimal device design. Intuitively, one might expect that if the constraints are very tight, the optimal device shape is the same regardless of incorporating or not the constrained control at the geometry optimization stage. However, this paper tests the hypothesis that the imposition of constraints will limit the control influence on the optimal device shape. PSOC, LC and passive control (PC) are considered in this study. In addition, constrained versions of LC and PC are presented.

Keywords: wave energy; power optimization; optimal geometry; control; constraints

1. Introduction

Wave energy technology development is at a relatively early stage of maturity. A wide variety of wave energy converters (WECs) with many different operating principles have been proposed and tested in the sea [1], but there are a few commercially-available devices. The levelized cost estimates of wave energy, *i.e.*, the production cost of an energy unit (1 kWh), is still higher than the estimated costs of non-renewable sources (e.g., pulverized fuel and nuclear) and other renewable sources (e.g., onshore and offshore wind) [2]. Thus, there is a corresponding "fertile field" for tools and techniques able to address improvements in the economic cost of wave energy.

Many aspects of WEC design and operation can be affected by dynamic analysis and control system technology, including maximization of energy extraction from waves and optimization of the

energy conversion in the power take-off (PTO) system [3]. Such tools can play a fundamental role in improving the performance of WECs and allowing the wave energy conversion to be performed as economically as possible to minimize the delivered energy cost.

Aiming to improve wave energy extraction, a number of studies have been carried out on device geometry optimization of WECs [4–8] and on control strategies for optimising the wave energy absorption; see, e.g., [9–12]. The WEC geometry is usually designed for the prevailing sea conditions in a particular location, and the control techniques are subsequently used to improve the energy conversion performance of the device for sea states other than the design sea state. However, particular control strategies, subsequently employed and while doing their best to broaden the frequency response or the response amplitude operator (RAO) across the active frequency range, can be limited in capability to produce an overall optimal system.

Recently, [13] has shown that different optimal geometries are obtained depending on the type of control strategy that is employed at the design optimization stage of the WEC, where no device amplitude and force constraints are considered. An optimal geometry obtained with latching control (LC) is highly control dependent and can shorten the original natural resonance period of the device. The optimal geometry obtained with a declutching-controlled device is slightly different from an uncontrolled device, and its resonance period is marginally longer than the uncontrolled case. In addition, a pseudo-spectral optimal control (PSOC) optimizes the wave energy absorption regardless of the geometry of the device. For the PSOC, nearly the same amount of power can be obtained, no matter whether the control design is incorporated at the geometry optimization stage or not. However, constraints in the amplitude of the body motion, and PTO force constraints, may influence the optimal geometry dependence, especially in the PSOC case, which results in more exaggerated motion of the body and requires higher PTO forces than the latching or declutching strategies.

Most WECs are subject to constraints on the PTO system, such as the PTO stroke length and the maximum force that the PTO can tolerate. Thus, for practical application studies, the physical constraints of the PTO system should be taken into account. The objective of this paper is to verify the impact of device motion and PTO force constraints on the control-informed geometry optimization of WECs.

We assume that the PTO stroke length is related to the amplitude of the body motion and that the amplitude of the motion cannot exceed the draught of the body. In addition, different limits are considered for the constraints in the PTO force. The following control strategies are used here: passive control (PC), LC and PSOC.

2. Energy from Sea Waves

In order to absorb energy from the waves, an oscillating body must be equipped with a PTO system, which allows the production of usable energy. The process of energy conversion is based on the body motion (in one or more degrees of freedom) as a response to incoming waves, and then, the kinetic energy is transferred into electrical energy either by means of a hydraulic intermediate stage or directly by a linear generator, depending on the PTO mechanism. Here, we consider a generic WEC with a generic PTO system. The WEC is represented as a truncated vertical cylinder with a wetted surface defined by a draught d and a radius r, as is illustrated by Figure 1.

2.1. Mathematical Model of Oscillating Bodies

Linear hydrodynamic theory and heave oscillatory motion of the cylinder are assumed. In such a case, the motion of the floating body can be described by Cummins' equation [14]:

$$[M + M_{\mathrm{r}}(\infty)]\ddot{x}(t) + \int_0^{\infty} K(t-\tau)\dot{x}(\tau)\mathrm{d}\tau + S_{\mathrm{h}}\, x(t) = \mathrm{f_e}(t) + \mathrm{f_p}(t) \tag{1}$$

where $x(t)$ is the vertical position of the body, M is the body mass, $M_{\mathrm{r}}(\infty)$ is the infinite-frequency added mass coefficient, defined with the added mass asymptotic value at infinite frequency, S_{h} is the

hydrodynamic stiffness coefficient, $f_e(t)$ is the wave excitation force and $f_p(t)$ is the force applied by the PTO mechanism. The kernel of the convolution term, $K(t-\tau)$, is known as the fluid memory term and expressed as [14]:

$$K(t-\tau) = \frac{2}{\pi}\int_0^\infty B_r(\omega)\cos[\omega(t-\tau)]d\omega \tag{2}$$

where $B_r(\omega)$ is the radiation damping coefficient and ω is the wave frequency. Assuming the body is floating in equilibrium, the body mass is equal to the mass of the displaced water in free flotation, that is:

$$M = \rho\,\pi r^2 d \tag{3}$$

where ρ is the water density. Furthermore, the natural resonant period of the device is defined as:

$$T_r = 2\pi\sqrt{\frac{M + M_r(\infty)}{S_h}} \tag{4}$$

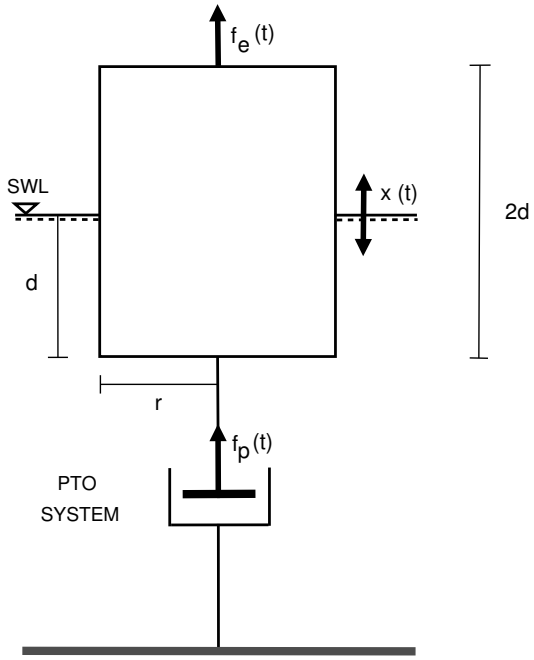

Figure 1. Schematic of the generic heaving floating body. PTO: power take-off.

The excitation force is calculated as $f_e(t) = \mathcal{F}^{-1}\{F_e(\omega)\eta(\omega)\}$, where $\eta(\omega)$ is the Fourier transform of the wave elevation and $F_e(\omega)$ is the excitation force transfer function.

The extracted energy and the mean extracted power by the WEC over a time range T_0 are, respectively, calculated as:

$$E_a = -\int_0^{T_0} \dot{x}(t) f_p(t) dt \tag{5}$$

$$P_a = \frac{E_a}{T_0} \tag{6}$$

where f_p is the force applied by the PTO system and $\dot{x}$ is the velocity of the body.

2.2. Upper Bounds for Wave Power Absorption

By virtue of the conservation of energy, WECs must interact with the waves and reduce the amount of energy present in the sea. The device must be able to generate waves, which interfere destructively with the sea waves [15]. For sinusoidal incident waves, the optimum destructive interference occurs when two optimum conditions for the body oscillation (phase and amplitude conditions) are fulfilled. The optimum phase condition is verified when the body velocity oscillates in phase with the wave excitation force, and the optimum amplitude condition implies that the resistive load of the PTO force must equal the hydrodynamic damping coefficient at the incident wave frequency [15].

The maximum power that can be absorbed by an oscillating body, or the optimum destructive interference, corresponds to [16–18]:

$$P_{max} = \frac{J\lambda}{2\pi} \tag{7}$$

where J is the power level of a sinusoidal plane wave and λ is the wavelength. On deep water, $\lambda = (g/2\pi)$ and $J = \rho g^2 T H^2/(32\pi)$, where g is the acceleration due to gravity, H is the wave height and T is the wave period. Thus, the upper limit for the absorbed power P_a is given by [19]:

$$P_a < P_A \equiv c_\infty T^3 H^2 \tag{8}$$

where $c_\infty = \rho(g/\pi^3)/128$ for an incident sinusoidal plane wave interfering with a ring-shaped outgoing wave from a heaving axisymmetric body [19].

Taking into account the physical limitations of the body, Budal [20] presented an upper bound (P_B) of the absorbed wave power by an immersed oscillating volume V_o,

$$P_B \equiv c_0 \frac{V_o H}{T} \tag{9}$$

where $c_0 = \pi\rho g/4$.

For a practical WEC, the converted power is necessarily below the upper bounds P_A and P_B. However, it does not mean that the whole region between these bounds is allowed [19]. The physical limits of the PTO, which are specific to the PTO itself, should also be taken into account for practical application studies.

3. Control-Informed Geometry Optimization

The overall optimization of the WEC consists of determining the radius r and draught d of the cylinder that maximizes the average absorbed power P_a in Equation (6), informed by the control system employed. The following control strategies are applied: PC, LC and PSOC.

Physical limitations of the WEC are taken into account by introducing constraints on the motion of the body. In particular, an oscillation amplitude constraint is introduced to reflect the finite excursion of the body, and a constraint on the PTO force is also introduced, indicating the maximum force that the PTO can tolerate. For the device motion constraints, the amplitude of the body motion cannot exceed the draught of the body. Thus, the oscillation amplitude constraint is defined as:

$$|x(t)| \leq k_C\, d \tag{10}$$

where k_C is a dimensionless constant, and $0 < k_C < 1$. In addition, the PTO force constraint is defined as:

$$|f_p(t)| \leq F_C \tag{11}$$

where F_C (in N) represents the physical limitation of the PTO system.

3.1. Control Methods

3.1.1. Passive Control

PC consists of varying the damping coefficient of the PTO force for a given sea state. If we consider a generic PTO system with a linear damper (coefficient $B_p \in R_+$), then the PTO force is given by:

$$f_p(t) = -B_p \dot{x}(t) \tag{12}$$

where $\dot{x}(t)$ is the vertical velocity of the body.

Assuming the wave excitation force is known completely over the interval T_0, the motion of the body can be estimated. Thus, the PTO coefficient B_p is initially tuned as:

$$B_p \equiv B_{pc,opt} = \sqrt{(B_r(\omega))^2 + (\omega(M + M_r(\omega)) - S_h/\omega)^2} \tag{13}$$

which represents optimal linear damping when the body is subjected to incident regular waves [15]. Polychromatic waves are not defined by a single frequency, so a frequency that best characterizes the wave spectrum should be selected. Here, B_p is tuned to the peak frequency of the wave spectrum (ω_p) for each sea state. Notice that tuning B_p to the peak frequency of the spectrum is a sub-optimal approach. An optimal approach where B_p is time varying and obtained through a nonlinear model predictive controller is presented in [21].

We define the maximum amplitude of the body motion over the time interval T_0 as:

$$x_m(B_p) = \max|x(t)|_{T_0} \tag{14}$$

if $x_m(B_p)$ does not exceed the allowed limits, defined by Equation (10), with B_p defined by Equation (13), then $B_p = B_{pc,opt}$. Otherwise, the following optimization problem is defined to find the damping B_p: Find the optimal damping B_p that minimizes the function , defined as:

$$(B_p) = k_C\, d - x_m(B_p) \quad s.t. \quad B_p > B_{pc,opt} \tag{15}$$

Here, the method of bisection [22] is used for solving Equation (15).

3.1.2. Latching Control

The principle of LC is to lock the motion of the body at the moment its velocity vanishes and to wait for a favourable situation to release the body again. As a result, the body velocity is forced to be in phase with the wave excitation force. The determination of the time that the body is locked (latching duration, T_L) is the problem to be solved. Figure 2 illustrates the evolution of the system variables under LC.

LC "slows down" the natural response of the device when the wave period is longer than the device period, in order to force the velocity of the body and the excitation force to reach their extrema (maxima or minima) at the same time.

The latching time can be determined semi-analytically for regular waves [23,24]. However, for polychromatic waves, the concept of phase between excitation force and velocity is not well defined, in which case the optimization of the latching duration does not return a unique solution [23]. In this case, the latching duration (or equivalently, the unlatching time) can be optimized to synchronize the peak of the velocity with the peak of the excitation force [25] or to maximize the absorbed power [9]. In addition, a number of different strategies have been proposed to determine the best unlatching time for polychromatic waves; see, e.g., [26–32]. In this study, the body is unlatched at the instant when the excitation force passes a chosen threshold (threshold unlatching [30]). Here, we choose zero as the threshold value. In [31], the authors verify the influence of the threshold unlatching time, the

PTO damping coefficient and the mass ratio of a generic two-body WEC on the LC efficiency for a given annual wave climate.

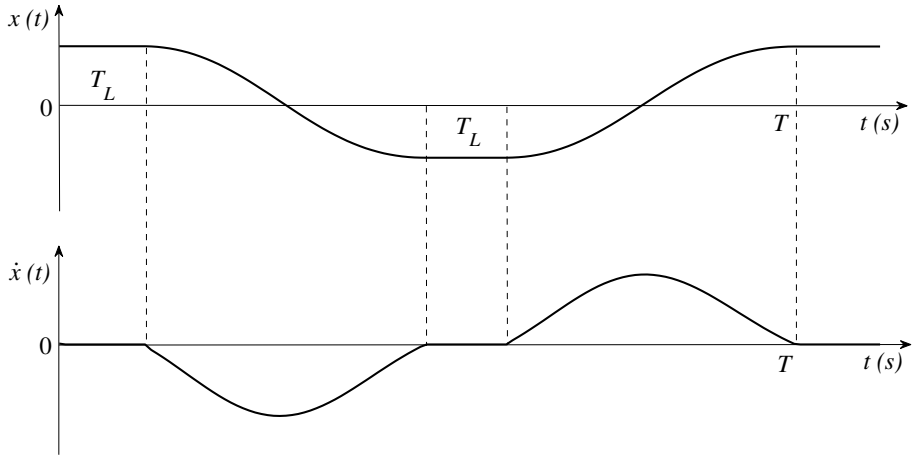

Figure 2. System variables under latching control (LC).

The PTO force is defined by Equation (12) for the instants the PTO is on. To further optimize the wave energy absorption, an optimal PTO damping can also be determined for the LC. In this case,

$$B_{\mathrm{p}} \equiv B_{\mathrm{lc,opt}} = D_{\mathrm{m}}\, M \tag{16}$$

where $0.05 < D_{\mathrm{m}} < 2.5$, and the problem to be solved is to determine the coefficient D_{m}, which optimizes the absorbed power for a specific geometry and sea state.

If x_{m} in Equation (14) does not exceed the allowed limits, defined by Equation (10), with B_{p} defined by Equation (16), then $B_{\mathrm{p}} = B_{\mathrm{lc,opt}}$. Otherwise, the same optimization problem defined for finding the optimal damping for the PC is defined for the LC. In this case, Equation (15) is subject to $B_{\mathrm{p}} > B_{\mathrm{lc,opt}}$. The method of bisection is also used to calculate the optimal B_{p} due to the motion constraint. Notice that for both the PC and LC, the PTO force constraint is implemented as a saturation. However, this is only a theoretical approach, since the body motion is also a function of the wave excitation force, which is an external force that cannot be manipulated. The implementation of saturation on the force signals of a real WEC is not physically possible.

3.1.3. Pseudo-Spectral Optimal Control

The control problem for the PSOC is defined as follows: to find the optimal profile for the PTO force that maximizes the total energy absorbed (Equation (5)) over a time interval T_0, subjected to the equation of motion (Equation (1)) and the physical constraints (Equations (10) and (11)).

For this purpose, the control problem is discretised by approximating the velocity and the PTO force with a linear combination of basis functions. Such a combination results in a finite dimension optimization problem. Following the procedure from [33,34], trigonometric functions are chosen as basis functions. Then, the PTO force and the velocity are, respectively, approximated with the truncated zero-mean Fourier series:

$$\dot{x}(t) \approx \sum_{k=1}^{N/2} x_{2\mathrm{k}}^{\mathrm{c}} \cos(k\omega_0 t) + x_{2\mathrm{k}}^{\mathrm{s}} \sin(k\omega_0 t) = \Phi(t)\, \hat{\boldsymbol{x}}_2 \tag{17}$$

$$\mathrm{f_p}(t) \approx \sum_{k=1}^{N/2} u_{\mathrm{k}}^{\mathrm{c}} \cos(k\omega_0 t) + u_{\mathrm{k}}^{\mathrm{s}} \sin(k\omega_0 t) = \Phi(t)\, \hat{\boldsymbol{u}} \tag{18}$$

where ω_0 is the fundamental frequency of the Fourier series, N is the total number of components and $\Phi(t) = \left[\cos(\omega_0 t), \sin(\omega_0 t), \ldots \cos(\frac{N}{2}\omega_0 t), \sin(\frac{N}{2}\omega_0 t)\right]$. The best approximation of the solution for the equation of motion (Equation (1)) is sought by applying the Galerkin method (see [33,34] for more details), and the result is the linear system:

$$\boldsymbol{G}\hat{\boldsymbol{x}}_2 = \hat{\boldsymbol{u}} + \hat{\boldsymbol{e}} \tag{19}$$

where $\hat{\boldsymbol{x}}_2$, $\hat{\boldsymbol{u}}$, $\hat{\boldsymbol{e}}$ are, respectively, the vectors of the Fourier coefficients of the velocity, PTO force and excitation force and $\boldsymbol{G}$ is the matrix of hydrodynamical coefficients of the system. The set of vectors are arranged as:

$$\hat{\boldsymbol{x}}_2 = \left[x_{21}^{\mathrm{c}}, x_{21}^{\mathrm{s}}, x_{22}^{\mathrm{c}}, x_{22}^{\mathrm{s}}, \ldots, x_{2\frac{N}{2}}^{\mathrm{c}}, x_{2\frac{N}{2}}^{\mathrm{s}}\right]^T$$
$$\hat{\boldsymbol{u}} = \left[u_1^{\mathrm{c}}, u_1^{\mathrm{s}}, u_2^{\mathrm{c}}, u_2^{\mathrm{s}}, \ldots, u_{\frac{N}{2}}^{\mathrm{c}}, u_{\frac{N}{2}}^{\mathrm{s}}\right]^T$$
$$\hat{\boldsymbol{e}} = \left[e_1^{\mathrm{c}}, e_1^{\mathrm{s}}, e_2^{\mathrm{c}}, e_2^{\mathrm{s}}, \ldots, e_{\frac{N}{2}}^{\mathrm{c}}, e_{\frac{N}{2}}^{\mathrm{s}}\right]^T$$

The matrix $\boldsymbol{G} \in \mathrm{R}^{\mathrm{N}\times\mathrm{N}}$ is defined as:

$$\boldsymbol{G} = \begin{bmatrix} \mathrm{D}_1 & \mathrm{C}_1 & 0 & \cdots & 0 & 0 \\ -\mathrm{C}_1 & \mathrm{D}_1 & 0 & \cdots & 0 & 0 \\ 0 & 0 & \ddots & & \vdots & \vdots \\ \vdots & \vdots & & \ddots & 0 & 0 \\ 0 & 0 & 0 & 0 & \mathrm{D}_{N/2} & \mathrm{C}_{N/2} \\ 0 & 0 & 0 & 0 & -\mathrm{C}_{N/2} & \mathrm{D}_{N/2} \end{bmatrix}$$

with:

$$\mathrm{D_k} = B_{\mathrm{r,k}}(k\omega_0)\text{, and}$$
$$\mathrm{C_k} = k\omega_0\left(M + M_{\mathrm{r,k}}(k\omega_0)\right) - \mathrm{S_{h,k}}/(k\omega_0)$$

The vector of the Fourier coefficients of the position can be expressed as [33]:

$$\hat{\boldsymbol{x}}_1 = D_\phi^{-1}\hat{\boldsymbol{x}}_2 \tag{20}$$

where $D_\phi \in \mathrm{R}^{\mathrm{N}\times\mathrm{N}}$ is the differentiation matrix. Each block $\boldsymbol{D}_\phi^{\mathrm{k}}$ for $k = 1, \ldots, N/2$ is:

$$\boldsymbol{D}_\phi^{\mathrm{k}} = \begin{bmatrix} 0 & k\omega_0 \\ -k\omega_0 & 0 \end{bmatrix} \tag{21}$$

The physical limitations in Equations (10) and (11) are also discretised. Following [33], the approximated position and force constraints are enforced only at a set of specific time instants $\{t_{\mathrm{k}}\}_{k=0}^{N_{\mathrm{c}}}$. The resulting amplitude and force constraint are respectively approximated by the linear inequalities:

$$\begin{bmatrix} \boldsymbol{\Theta} \\ -\boldsymbol{\Theta} \end{bmatrix} \hat{\boldsymbol{x}}_1 \leq \mathbf{1}_{2(N_{\mathrm{c}}+1)\times 1}\, k_{\mathrm{C}}\, d \tag{22}$$

$$\begin{bmatrix} \boldsymbol{\Theta} \\ -\boldsymbol{\Theta} \end{bmatrix} \hat{\boldsymbol{u}} \leq \mathbf{1}_{2(N_{\mathrm{c}}+1)\times 1}\, F_{\mathrm{C}} \tag{23}$$

where $\mathbf{1}_{2(N_{\mathrm{c}}+1)\times 1}$ is the vector of all ones of size $2(N_{\mathrm{c}}+1)$, and $\boldsymbol{\Theta} = [\Phi_0, \Phi_1, \ldots, \Phi_{N_{\mathrm{c}}}]^T$. The motion inequality constraint in Equation (22) can be expressed as a function of $\hat{\boldsymbol{u}}$ using Equations (19) and (20):

$$\begin{bmatrix} \boldsymbol{\Theta} \\ -\boldsymbol{\Theta} \end{bmatrix} D_{\phi}^{-1} \boldsymbol{G}^{-1} \hat{\boldsymbol{u}} \leq \mathbf{1}_{2(N_c+1)\times 1}\, k_C\, d - D_{\phi}^{-1} \boldsymbol{G}^{-1} \hat{\boldsymbol{e}} \tag{24}$$

Assuming the wave excitation force is known completely over the time interval T_0 and $\mathbf{G}$ is nonsingular, the vector of the optimal PTO force $\hat{\boldsymbol{u}}^*$ is obtained by solving the following optimization problem [33]:

$$\hat{\boldsymbol{u}}^* = \arg\max_{\hat{\boldsymbol{u}}} (-\hat{\boldsymbol{u}}^T \boldsymbol{G}^{-1} \hat{\boldsymbol{u}} - \hat{\boldsymbol{u}}^T \boldsymbol{G}^{-1} \hat{\boldsymbol{e}}) \tag{25}$$

subject to the linear inequality constraints on the PTO force (Equation (23)) and oscillation amplitude (Equation (24)). More details on how to solve the energy optimization problem subject to device motion and force constraints can be obtained in [33].

All of the constrained control strategies considered in this paper require the wave excitation force to be known completely over the time interval T_0 to optimize B_p (PC or LC) or to determine the optimal PTO force (PSOC). In addition, the optimal power absorption by the PSOC may require a PTO that is able to supply power during part of the wave cycle (reactive power), which places particular demands on PTO systems.

4. Simulations Results

4.1. Simulation Parameters

The optimal geometries informed by the control system employed (PC, LC or PSOC) are determined via simulations with a complete set of possible values of radius r and draught d, in which 153 different cylinders are considered. As a result, a clear overview of the mapping between the absorbed power P_a and the optimization parameters can be observed. The ranges of both the radii and draughts goes from 2 m to 18 m, in steps of 1 m (radius) and 2 m (draught). The coefficients $F_e(\omega)$, $B_r(\omega)$, $M_r(\infty)$ and S_h for all of the cylinders are computed using the boundary element solver WAMIT [35]. In Equations (1), (2) and (4), all of the hydrodynamic quantities are represented in the dimensional form, following guidelines from [35].

Polychromatic waves are considered for the control-informed geometric optimization study of the WEC subject to constraints. The polychromatic waves are calculated as a linear combination of monochromatic waves using a Bretschneider spectral envelope, defined by the significant wave height $H_s = 1.8$ m, peak period $T_p = 7.4$ s and random phases. Phases were pre-computed once in order to be exactly the same for every simulation.

4.1.1. Passive Control and Latching Control Parameters

For the PC and the LC strategies, the fourth-order Runge–Kutta method is adopted for simulating the equation of motion (Equation (1)). The time step used is 0.1 s, and the time interval T_0 is set to 1200 s, which is the usual recording time used to obtain real statistical values of a wave field and to characterize a sea state [36].

The PTO damping coefficients were pre-computed for each one of the geometries following the procedure described in Sections 3.1.1 and 3.1.2. The initial interval chosen for the bisection method is defined as: $[B_{pc,opt}, 5B_{pc,opt}]$ for PC or $[B_{lc,opt}, 5B_{lc,opt}]$ for LC. The bisection algorithm stops when the difference between two consecutive damping values is less than or equal to 1000 kg/s. Figure 3 shows the PTO damping coefficients for PC and LC with the studied cylinders and the defined sea state.

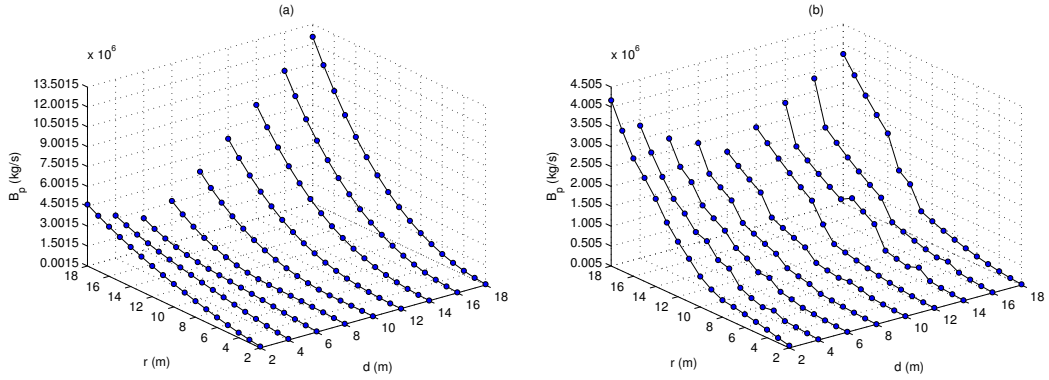

Figure 3. PTO damping coefficients when $k_C = 0.75$ for (**a**) passive control (PC) and (**b**) LC.

4.1.2. Pseudo-Spectral Optimal Control Parameters

In the PSOC, the optimal control problem is discretized by approximating the velocity of the body and the PTO force with truncated zero-mean Fourier series. Then, the solution of the linear system (Equation (19)) represents the steady-state solution of the equation of motion (Equation (1)), and the time interval T_0 is defined by the fundamental frequency of the Fourier series, that is $T_0 = 2\pi/\omega_0$. For regular waves, $\omega_0 = \omega$. For panchromatic waves, a simulation study has been done to determine ω_0 for the sea state $H_s = 1.8$ m and $T_p = 7.4$ s. Figure 4 shows the normalized absorbed power by the WEC as a function of T_0 (Figure 4a) and as a function of the number of frequencies (Figure 4b). The normalized absorbed power is calculated as P_a/P_a^*, where P_a^* is the average absorbed power for $T_0 = 1200$ s. In Figure 4a, the number of frequencies for each one of the simulations is defined as $N = 2T_0/T_p$. It can be noted that for $T_0 > 60$ s, the power ratio converges to one. For panchromatic waves, the simulation parameters are set as: $N = 128$ and $\omega_0 = 0.0304$ rad/s.

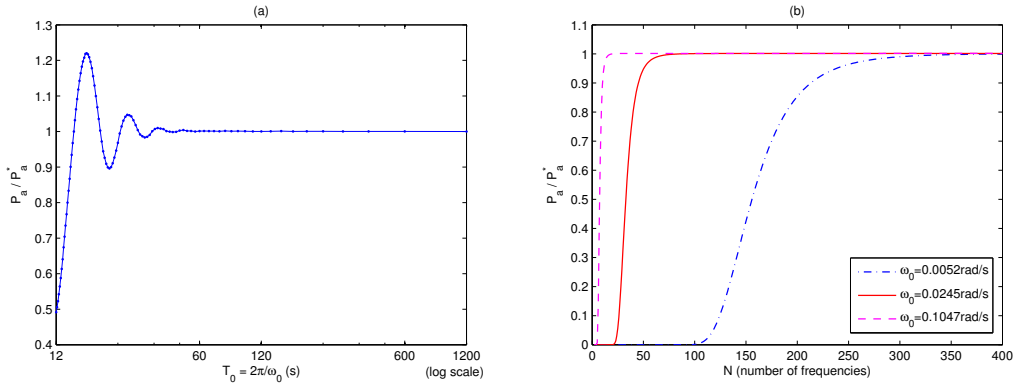

Figure 4. Normalized absorbed power by the cylinder ($r = 5$ m; $d = 10$ m) as a function of (**a**) the time interval T_0 and (**b**) the number of components of the Fourier series. Panchromatic waves.

4.1.3. Budal Diagram

Figure 5 shows the Budal diagram with the two upper bounds for wave energy absorption (P_A and P_B) for a geometry with $r = 5$ m and $d = 10$ m and the power absorbed by the same geometry when different control strategies and PTO constraints are adopted. It can be noted that the unconstrained PC and LC result in absorbed powers below the allowed regions, but the unconstrained PSOC results in about the same power as suggested by the upper bound P_A. Thus, we have used the upper bounds curves in Figure 5 to define the PTO force limits (F_C). After trial and error, we verify that for $k_C = 0.75$ and $F_C \leq 3500$ kN, the absorbed power by the PSOC is inside the allowed region defined by curves P_A and P_B.

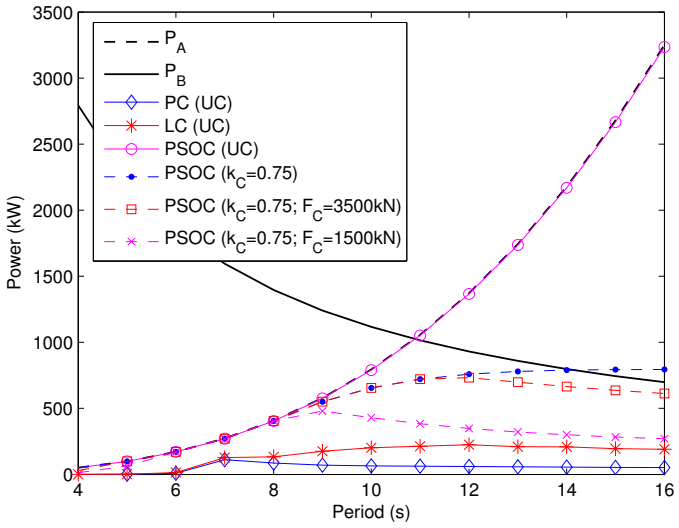

Figure 5. Two upper bounds (P_A and P_B) for the power that can be absorbed from a sinusoidal wave with $H = 1.8\,\text{m}$ and power absorbed by the cylinder ($r = 5\,\text{m}$; $d = 10\,\text{m}$) when different control strategies and constraints are employed for it.

4.2. Optimal Geometries

Figures 6 – 8 illustrate the variation of the absorbed power P_a for different values of r and d for each of three control methods (PC, LC and PSOC). Figures 6 – 8 also show the level curves of P_a under the surface plot and the optimal cylinder parameters, which are identified by the symbol "$*$". In order to compare different scenarios for the optimal geometries informed by the control system employed, the simulations were run without any constraints on the oscillation amplitude of the body or PTO force (Figure 6), with amplitude constraints only (Figure 7) and with both oscillation amplitude constraints and PTO force constraints (Figure 8). Table 1 shows the relative size of the various optimized devices when the constrained control strategies are subject to different PTO constraints. The first line shows the optimal geometries for the cases when the PTO is not constrained (NC). Overall, 11 different geometries are obtained for the considered scenarios.

By comparing Figure 6a with Figure 7a, it can be noted that the oscillation amplitude constraints have no effect over the variation of the absorbed power for PC. Only when the PTO force limits are lower than 500 kN ($F_C < 500\,\text{kN}$) are the optimal geometries smaller than the case when the PTO force is unconstrained, or the PTO limits are not very constraining for PC ($F_C \geq 1500\,\text{kN}$). For LC, the amplitude constraint slightly modifies the absorbed power for the smallest geometries, but the optimal geometries are still the same, as is illustrated by Figures 6b and 7b. The optimal geometry becomes different only when the PTO force is restricted to 250 kN (Table 1).

For the PSOC cases, the amplitude constraint has an effect on the power absorbed for the smallest bodies (Figure 7c), and the PTO force constraint affects the power absorbed by the biggest bodies (Figure 8c). An interesting effect is noticed here for the optimal geometries: the cylinders are flat geometries when the PTO force is unconstrained or set to more relaxed limits (e.g., $F_C = 3500$ kN, which is about 82% of the maximum value of the PTO force in the unconstrained case). Nonetheless, the optimal geometries are slender cylinders when conservative PTO limits are imposed (e.g., $F_C = 500$ kN, which is about 12% of the maximum value of the PTO force in the unconstrained case). Notice that a zoom of the flat region has been included in Figure 7c to better illustrate the variation of the absorbed power for such a region.

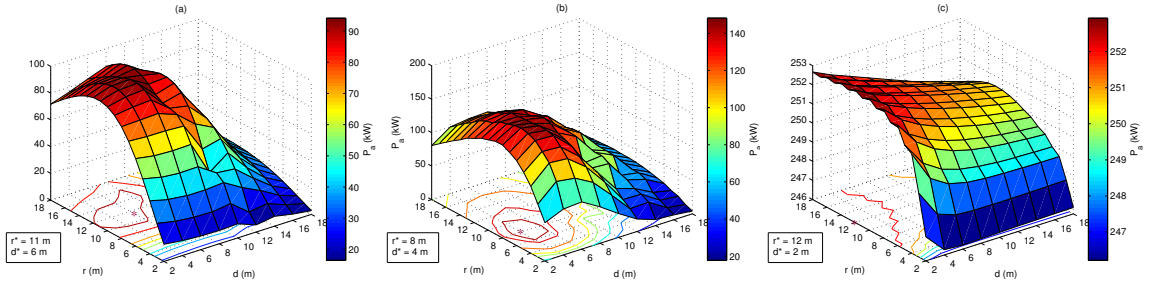

Figure 6. Absorbed power by the cylinders without constraints: (**a**) PC, (**b**) LC and (**c**) pseudo-spectral optimal control (PSOC).

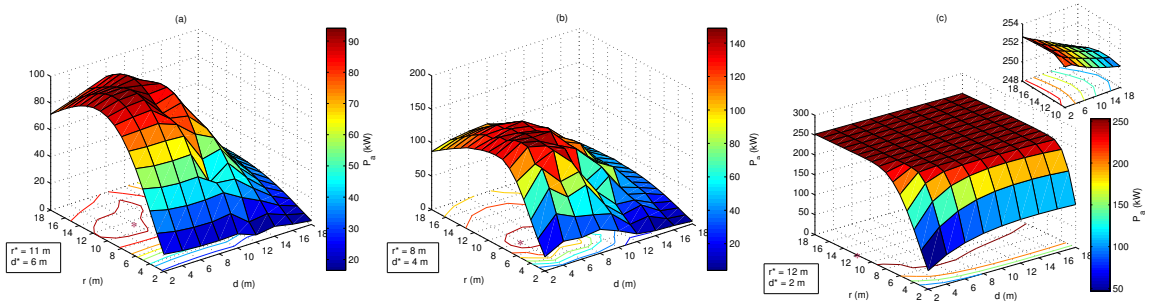

Figure 7. Absorbed power by the cylinders with oscillation amplitude constraints ($k_C = 0.75$) and without force constraints: (**a**) PC, (**b**) LC and (**c**) PSOC.

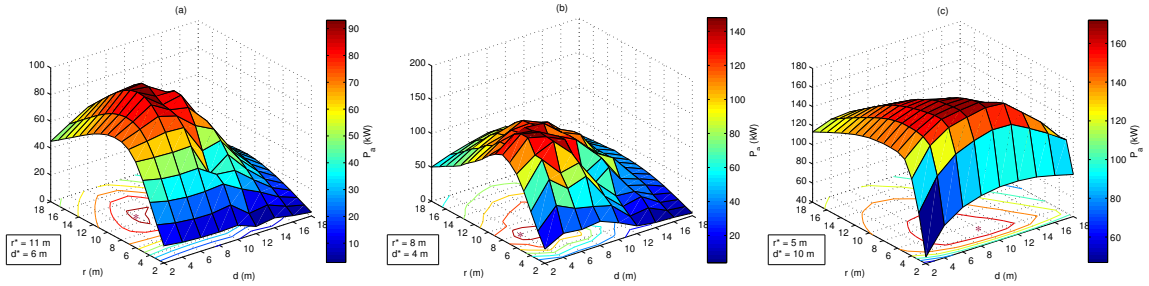

Figure 8. Absorbed power by the cylinders with oscillation amplitude constraints ($k_C = 0.75$) and force constraints ($F_C = 500$ kN): (**a**) PC, (**b**) LC and (**c**) PSOC.

Table 1. Optimal values of r (m), d (m) and T_r (s) of the cylinders for different constrained control strategies. The PTO is subject to device motion constraints (defined by $k_C\,d$) and force constraints (defined by F_C in kN). The first line shows the optimal parameters for the unconstrained control cases. NC, not constrained.

k_C	F_C	PC				LC				PSOC			
		Geometry	r^*	d^*	T_r^*	**Geometry**	r^*	d^*	T_r^*	**Geometry**	r^*	d^*	T_r^*
NC	NC	A	11	6	7.06	B	8	4	5.91	C	12	2	5.78
0.75	3500		11	6	7.06		8	4	5.91		12	2	5.78
0.75	1500		11	6	7.06		8	4	5.91	D	7	6	6.43
0.75	500		11	6	7.06		8	4	5.91	E	5	10	7.32
0.75	250	F	9	8	7.37	G	6	6	6.27	H	4	10	7.16
0.75	125	I	8	8	7.22	J	5	6	6.08	K	3	12	7.55

It can be noted that different optimal geometries are obtained depending on the control strategy employed and on the constraints, but overall, tight PTO force constraints result in optimal

geometries with smaller radii, bigger draughts and longer resonant periods than relaxed PTO limits or unconstrained cases. Figure 9 illustrates the effect of the constraints on the RAO of the PSOC, when geometries C and K are adopted, respectively, for $F_C = 3500$ kN and $F_C = 125$ kN. Figure 9 shows that a tight PTO force constraint results in a large peak in the RAO plot and that a relaxed constraint results in a low peak and a large plateau, as is expected, respectively, for geometries with big draughts (like geometry K) and geometries with small draughts (like geometry C).

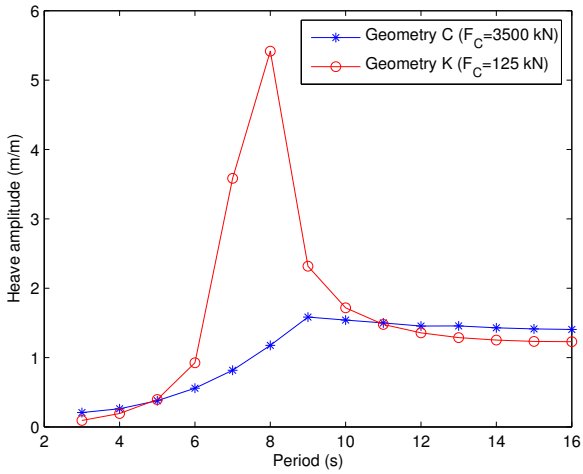

Figure 9. Response amplitude operator (RAO) for optimal geometries with constrained PSOC. PTO constraints: $k_C = 0.75$, and the force constraints are $F_C = 3500$ kN (for geometry C) and $F_C = 125$ kN (for geometry K).

4.3. Discussion

Table 1 shows that the geometries designed with unconstrained control are the same as the geometries designed with constrained control when the limits of the PTO force are relaxed $F_C \geq 3500$ kN or when the force limits are $F_C \geq 500$ kN for the PC and LC (constraints are relatively inactive). To verify the impact of constrained control on the optimal shape of the device, firstly we compare the power absorbed by the WEC when two different geometries are used with a constrained controller. The first geometry is an optimal geometry designed for an unconstrained controller, and the second geometry is an optimal geometry designed for a constrained controller. The average power of the geometry designed for the unconstrained control is denoted by $P_{\text{geo\_uc}}$, and the average power of the geometry designed for constrained control is denoted by $P_{\text{geo\_cc}}$. Table 2 shows the average absorbed powers when different geometries are used with the constrained PC, LC and PSOC.

Table 2. Average absorbed power (kW) for various constrained control strategies with geometries that are designed with unconstrained control ($P_{\text{geo\_uc}}$) and geometries that are designed with constrained control ($P_{\text{geo\_cc}}$).

k_C	F_C (kN)	PC		LC		PSOC	
		$P_{\text{geo\_uc}}$	$P_{\text{geo\_cc}}$	$P_{\text{geo\_uc}}$	$P_{\text{geo\_cc}}$	$P_{\text{geo\_uc}}$	$P_{\text{geo\_cc}}$
0.75	3500	98.69	98.69	148.92	148.92	252.93	252.93
0.75	1500	98.69	98.69	148.92	148.92	239.08	245.51
0.75	500	98.69	98.69	148.07	148.07	134.90	171.98
0.75	250	62.01	76.14	114.65	137.65	78.34	121.15
0.75	125	33.77	51.30	64.75	100.30	42.39	81.77

It can be noted that if the force constraints are not very constraining (e.g., $F_c \geq 1500$), the effect of considering the constraints in the control-informed optimal design is null or minimal. However, more constraining limits in the PTO force do have an impact on the optimal geometry and, consequently,

on the absorbed power. For instance, when $k_C = 0.75$ and $F_C = 125$ kN, an improvement of 55% is obtained in the absorbed power if geometry J is adopted instead of B, for the LC. Note that geometry J is the optimal geometry for LC with $k_C = 0.75$ and $F_C = 125$ kN, as indicated by Table 1. Moreover, an improvement of up to 93% is obtained if geometry K is adopted instead of C for the PSOC.

In addition, our aim is to compare the power improvement of the constrained control-informed optimized geometries to the power improvement of the unconstrained control-informed optimized geometries. For this purpose, we follow the usual procedure of applying a control strategy to a geometry that was designed without the controller in place. Hence, we compare the performance (in terms of absorbed power) of applying such a control strategy to a geometry optimized with the same controller in place. Thus, we apply LC to geometries optimized when PC and LC were in place, and the same procedure is repeated applying PSOC to geometries optimized when PC and PSOC were in place. The average power absorbed by a geometry optimized for PC is denoted by P_{pc} and respectively by P_{lc} and P_{oc} for geometries optimized for LC and PSOC. The power improvement of the unconstrained control-informed optimized geometries is $P_{lc}/P_{pc} = 1.1896$ for LC and $P_{oc}/P_{pc} = 1.0044$ for PSOC. Figure 10 shows the ratios P_{lc}/P_{pc} and P_{oc}/P_{pc} for the constrained control cases where different PTO constraints are considered.

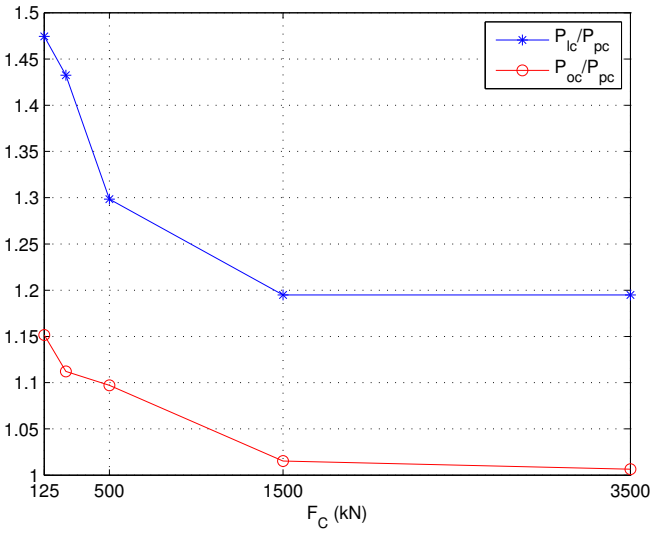

Figure 10. Ratio between the average absorbed power when two different optimal geometries are adopted for constrained LC (P_{lc}/P_{pc}) and PSOC (P_{oc}/P_{pc}). The PTO is subject to device motion constraints ($k_C = 0.75$) and force constraints (defined by F_C).

For the LC, it can be noted that when the constraints are more relaxed (e.g., $F_C \geq 1500$ kN), the impact of the constrained control strategy on the optimal shape of the device is the same impact of the unconstrained control case ($P_{lc}/P_{pc} = 1.1896$). Nonetheless, such an impact increases if more constraining limits are imposed on the PTO force, and a performance improvement of up to 82% can be obtained in the absorbed power, as is illustrated in Figure 10. For the PSOC, the impact of the control strategy on the optimal geometry is minimal if the controller is unconstrained or if the constraints are not very tight (e.g., $F_C = 3500$ kN), but the impact becomes significant if the constraints are tight. In this case, a performance improvement of up to 15% can be obtained, as is also illustrated in Figure 10.

A comparison of the power capture per unit volume for the cases when the same control strategies employed to the WEC (LC and PSOC) were in place at the geometry design stage with the cases where these strategies were not in place is illustrated in Figure 11, for $H_s = 1.8$ m, different peak periods and $k_C = 0.75$, $F_C = 1500$ kN. Figure 11a shows the power/volume ratio when LC

is employed to the WEC. It can be observed that the power/volume ratio for geometry B is up to 5.6 times larger than the ratio for geometry A, which is the optimal geometry for PC. A significant improvement is also observed in the ratio P_a/V_o for the PSOC strategy (Figure 11b) when geometry D is adopted. In this case, the power/volume ratio for geometry D is up to 2.7 times larger than the ratio for geometry A. However, it should be noted that the power capture per unit volume is not explicitly optimized in this study.

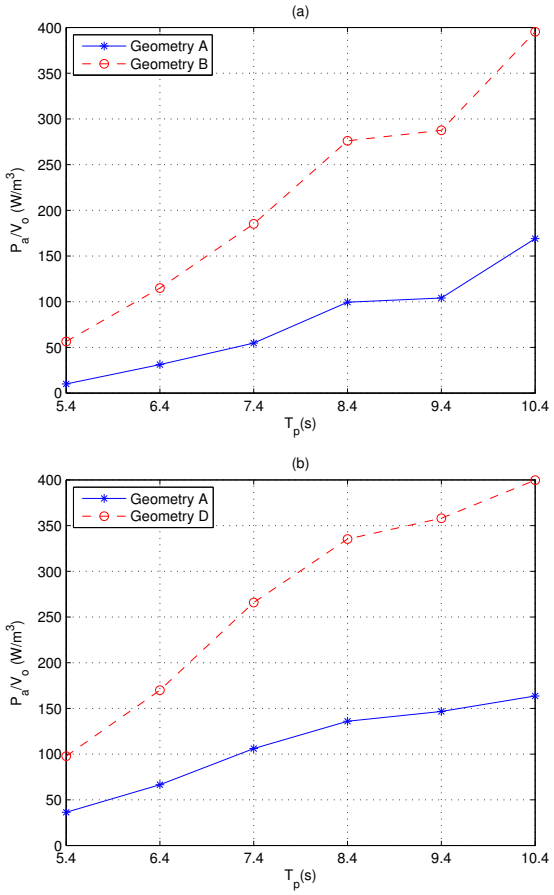

Figure 11. Power capture per unit volume when different geometries are adopted for constrained control: (**a**) LC and (**b**) PSOC. The PTO constraints are: $k_C = 0.75$, $F_C = 1500$ kN.

5. Conclusions

This paper has studied the effects of applying system constraints in the control-informed geometric optimization design of a WEC. Constraints in the amplitude of the body motion and PTO force constraints were considered. In contrast to what one might have expected, the effect of considering constraints in the control-informed optimized design of WECs is more significant when tight limits are adopted in the PTO force.

Different optimal geometries are obtained depending on the control strategy employed and on the constraints, but overall, tight PTO force constraints result in optimal geometries with smaller radii, bigger draughts and longer resonant periods than relaxed PTO limits or unconstrained cases. The optimal controller (PSOC) completely modifies the shape of the cylinder depending on the the maximum force that the PTO can tolerate: for relaxed force limits, the optimal cylinder is a flat geometry, and for very constraining limits, the cylinder becomes a slender geometry.

For the studied cases, the impact of the LC on the optimal device shape is already significant if the controller is unconstrained or if relaxed constraints are considered. An improvement of up to 19% can be obtained in the absorbed power when the optimization design stage of the geometry employs

the controller. Such an improvement increases for tighter constraints. In addition, the impact of the PSOC on the optimal device shape is minimal if the controller is unconstrained or if the constraints are not very tight (e.g., $F_c \geq 3500$ kN, which is about 82% of the maximum value of the PTO force in the unconstrained case). However, the impact of the PSOC on the optimal shape becomes significant if the constraints are tight.

In a real WEC environment, the study of the control-informed optimal geometry should consider the statistical sea states' occurrence of a specific site. Then, the best geometry can be defined after running simulations for a different set of wave parameters, e.g., significant wave height and peak period. The main focus of this paper is to prove that, for some sea states, the optimal (in terms of absorbed power) device geometry is sensitive to the control scheme employed, even under constrained control. The degree to which the control system influences the optimal geometry, and the nature of that influence, would likely vary between different sites and devices. Our main aim is to alert designers of the need to consider control at the device design stage.

For any comparative economic assessment of WECs, many aspects need to be taken into account, such as the device survivability and design specification and manufacturing, e.g., stroke length, PTO force limits, volume and type of material, *etc*. This study has shown that when constrained LC or PSOC are incorporated at the design stage of the geometry, the performance of the WEC in terms of absorbed power can improve, especially if the PTO force limits are tight.

Acknowledgements: This work was supported by the Science Foundation Ireland under Grant No. 12/RC/2302 for the Marine Renewable Energy Ireland (MaREI) Centre.

Author Contributions: The authors contributed equally to this work.

Conflicts of Interest: The authors declare no conflict of interest.

References

1. Falcão, A.F.O. Wave energy utilization: A review of the technologies. *Renew. Sustain. Energy Rev.* **2010**, *14*, 899–918.
2. Astariz, S.; Iglesias, G. The economics of wave energy: A review. *Renew. Sustain. Energy Rev.* **2015**, *45*, 397–408.
3. Ringwood, J.V.; Bacelli, G.; Fusco, F. Energy-Maximizing Control of Wave-Energy Converters. *IEEE Control Syst.* **2014**, *34*, 30–55.
4. Babarit, A.; Clément, A. Shape optimization of the SEAREV wave energy converter. In Proceedings of the IX World Renewable Energy Congress, Florence, Italy, 19–25 August 2006.
5. Alves, M.; Traylor, H.; Sarmento, A. Hydrodynamic Optimization of a Wave Energy Converter Using a Heave Motion Buoy. In Proceedings of the 7th European Wave and Tidal Energy Conference, Porto, Portugal, 11–13 September 2007.
6. McCabe, A.P.; Aggidis, G.A.; Widden, M.B. Optimizing the shape of a surge-and-pitch wave energy collector using a genetic algorithm. *Renew. Energy* **2010**, *35*, 2767–2775.
7. McCabe, A.P. Constrained optimization of the shape of a wave energy collector by genetic algorithm. *Renew. Energy* **2013**, *51*, 274–284.
8. Kurniawan, A.; Moan, T. Optimal Geometries for Wave Absorbers Oscillating About a Fixed Axis. *J. Ocean. Eng.* **2013**, *38*, 117–130.
9. Babarit, A.; Clément, A.H. Optimal latching control of a wave energy device in regular and irregular waves. *Appl. Ocean Res.* **2006**, *28*, 77–91.
10. Hals, J.; Falnes, J.; Moan, T. A Comparison of Selected Strategies for Adaptive Control of Wave Energy Converters. *J. Offshore Mech. Arct. Eng.* **2011**, *133*, doi:10.1115/1.4002735.
11. Garcia-Rosa, P.B.; Lizarralde, F.; Estefen, S.F. Optimization of the Wave Energy Absorption in Oscillating-Body Systems using Extremum Seeking Approach. In Proceedings of the 8th IFAC Conference on Control Applications in Marine Systems, Rostock, Germany, 15–17 September 2010; pp. 1011–106.
12. Fusco, F.; Ringwood, J.V. A simple and effective real-time controller for wave energy converters. *IEEE Trans. Sustain. Energy* **2013**, *4*, 21–30.

13. Garcia-Rosa, P.B.; Ringwood, J.V. On the Sensitivity of Optimal Wave Energy Device Geometry to the Energy Maximising Control System. *IEEE Trans. Sustain. Energy* **2015**, doi:10.1109/TSTE.2015.2423551.
14. Cummins, W.E. *The impulse response function and ship motions*; David Taylor Model Basin Washington DC: Washington, DC, USA, 1962.
15. Falnes, J. *Ocean Waves and Oscillating Systems: Linear Interaction including Wave-Energy Extraction*; Cambridge University Press: Cambridge, UK, 2002.
16. Budal, K.; Falnes, J. A Resonant Point Absorber of Ocean Waves. *Nature* **1975**, *256*, 478–479.
17. Newman, J.N. The Interaction of Stationary vessels with Regular Waves. In Proceedings of the 11th Symposium on Naval Hydrodynamics, London, UK, 28 March–2 April 1976; pp. 491–501.
18. Evans, D.V. A theory for wave-power absorption by oscillating bodies. *J. Fluid Mech.* **1976**, *77*, 1–25.
19. Falnes, J. A review of wave-energy extraction. *Mar. Struct.* **2007**, *20*, 185–201.
20. Budal, K.; Falnes, J. Interacting Point Absorbers with Controlled Motion. In *Power from Sea Waves*; Count, B.M., Ed.; Academic Press: London, UK, 1980; pp. 381–399.
21. Tom, N.; Yeung, R.W. Nonlinear Model Predictive Control Applied to a Generic Ocean-Wave Energy Extractor. *J. Offshore Mech. Arct. Eng.* **2014**, *136*, doi:10.1115/1.4027651.
22. Gill, P.E.; Murray, W.; Wright, M.H. *Practical Optimization*; Academic Press: New York, NY, USA, 1981.
23. Babarit, A.; Duclos, G.; Clément, A.H. Comparison of latching strategies for a heaving wave energy device in random sea. *Appl. Ocean Res.* **2004**, *26*, 227–238.
24. Nolan, G.; Ringwood, J.V.; Butler, W.E.L.S. Optimal Damping Profiles for a Heaving Buoy Wave-Energy Converter. In Proceedings of the 15th International Society of Offshore and Polar Engineers Conference (ISOPE 2005), Seoul, Korea, 19–24 June 2005.
25. Hals, J.; Bjarte-Larsson, T.; Falnes, J. Optimum Reactive Control and Control by Latching of a Wave-Absorbing Semisubmerged Heaving Sphere. In Proceedings of the 21st International Conference on Offshore Mechanics and Arctic Engineering, Oslo, Norway, 23–28 June 2002; Volume 8, pp. 415–423.
26. Budal, K.; Falnes, J.; Iversen, L.C.; Lillebeken, P.M.; Oltedal, G.; Hals, T.; Onshus, T. The Norwegian wave-power buoy project. In Proceedings of the 2nd International Symposium on Wave Energy Utilization, Trondheim, Norway, 22–24 June 1982; pp. 323–344.
27. Eidsmoen, H. Tight-moored amplitude-limited heaving buoy wave energy converter with phase control. *Appl. Ocean Res.* **1998**, *20*, 157–161.
28. Korde, U.A. Phase control of floating bodies from an on-board reference. *Appl. Ocean Res.* **2001**, *23*, 251–262.
29. Falcão, A.F.O. Phase control through load control of oscillating-body wave energy converters with hydraulic PTO system. *Ocean Eng.* **2008**, *35*, 358–366.
30. Lopes, M.F.P.; Hals, J.; Gomes, R.P.F.; Moan, T.; Gato, L.M.C.; Falcão, A.F.O. Experimental and numerical investigation of non-predictive phase-control strategies for a point-absorbing wave energy converter. *Ocean Eng.* **2009**, *36*, 386–402.
31. Henriques, J.C.C.; Lopes, M.F.P.; Gomes, R.P.F.; Gato, L.M.C.; Falcão, A.F.O. On the annual wave energy absorption by two-body heaving WECs with latching control. *Renew. Energy* **2012**, *45*, 31–40.
32. Feng, Z.; Kerrigan, E.C. Latching control of wave energy converters using derivative-free optimization. In Proceedings of the IEEE 52nd Annual Conference on Decision and Control, Firenze, Italy, 10–13 December 2013; pp. 7474–7479.
33. Bacelli, G.; Ringwood, J.V. Numerical optimal control of wave energy converters. *IEEE Trans. Sustain. Energy* **2015**, *6*, 294–302.
34. Bacelli, G.; Ringwood, J.V.; Gilloteaux, J.C. A control system for a self-reacting point absorber wave energy converter subject to constraints. In Proceedings of the 18th IFAC World Congress, Milano, Italy, 28 August–2 September 2011; pp. 11387–11392.
35. *WAMIT User Manual*, Version 7.0; WAMIT, Inc.: Chestnut Hill, MA, USA, 2013.
36. Labeyrie, J. Stationary and Transient States of Random Seas. *Mar. Strucut.* **1990**, *3*, 43–58.